Bull. Mater. Sci. (2021)44:259
https://doi.org/10.1007/s12034-021-02550-y

Ferromagnetism in Gd-doped ZnO thin films mediated by defects

ARYA SUKUMARAN, N SIVANANTHAM, E VINOTH and N GOPALAKRISHNAN*
Thin Film Laboratory, Department of Physics, National Institute of Technology, Tiruchirappalli 620015, India
*Author for correspondence (ngk@nitt.edu)

MS received 5 April 2021; accepted 18 July 2021

Abstract. Defects play an inevitable role in controlling the optical and magnetic properties of ZnO. In this study, defects were introduced in gadolinium (Gd)-doped ZnO films by depositing in pure argon atmosphere. The pristine- and Gd-doped (0.05, 0.1 and 1 at%) films were deposited on Si(111) substrate by radio frequency magnetron sputtering at a substrate temperature of 450°C under Ar pressure of 0.02 mbar. Structural, morphological, chemical, optical and magnetic properties of the deposited films were studied by X-ray diffraction and Raman spectroscopy, atomic force microscopy, X-ray photoelectron spectroscopy, photoluminescence and vibrating sample magnetometer, respectively. It is confirmed that oxygen-deficient growth condition leads to the formation of oxygen vacancy (V_O^+) and zinc interstitial (Zn_i^+) defects in the films. It is shown that a critical amount of Zn_i^+ and V_O^+ along with the appropriate amount of Gd^{3+} ions are required to induce room temperature ferromagnetism in Gd-doped ZnO thin film deposited on Si(111) substrate. A possible mechanism has been proposed based on bound magnetic polaron model to explain the observed ferromagnetism.

Keywords. Gd-doped ZnO; radio frequency magnetron sputtering; room temperature ferromagnetism; bound magnetic polaron model; oxygen deficiency; defects.

1. Introduction

Materials whose properties rely on spin functionality are very important in the advancement of spintronics. Semiconductor spintronics is a field of dreams for the research community as it could pave the way for integrating spin-based mechanisms with current semiconductor technology. Lots of research is being carried out to induce ferromagnetism in nonmagnetic semiconductors, especially by doping 3d transition metals in semiconductors such as TiO_2 [1,2], ZnO [3,4], CeO_2 [5,6], SnO_2 [7,8] and GaN [9,10]. It is well known that, when doped with transition metal elements, certain semiconductors exhibit ferromagnetism, and are called diluted magnetic semiconductors (DMS). Among all the semiconductors, ZnO is a promising candidate for integrating multiple functions in a single system because of its direct and wide bandgap [11], large free exciton binding energy [11] and good thermal and chemical stability [12]. A large share of research in the field of DMS had been based on the use of 3d transition metals [3,4] as dopants for a long time. However, the interest has currently shifted to rare-earth (RE) [13–15], non-transition metals [16], anions such as nitrogen and carbon as dopants [17,18] and even undoped ZnO [19]. In all these cases, ZnO system is inferred to be exhibiting room temperature ferromagnetism (RTFM), depending on growth conditions and methods [20]. This has puzzled the scientific community ever since.

According to studies, an intriguing observation is that doping percentage higher than the percolation threshold of ZnO (18%) is not a prerequisite for RTFM [21]. The conventional super-exchange mechanism cannot explain this fact. The ferromagnetic double-exchange mechanism requires mixed cation valence, which is not a common feature in DMS [21]. Hence, the DMS systems must be explained by some other mechanism. A large body of literature is based on the mechanism where ferromagnetism is mediated by bound magnetic polarons (BMPs), which are related to the lattice defects in the system. Oxygen vacancy (V_O) based BMP model is widely discussed in the field of DMS [22–27]. There are some reports discussing zinc interstitial (Zn_i) and zinc vacancy (V_{Zn}) based BMP models as well. Recently, Ali *et al* [3] reported that V_{Zn} is responsible for RTFM in Cu-doped ZnO and Ag-doped ZnO [28]. Also, Wang *et al* [19] reported that RTFM in undoped ZnO is to be attributed to the presence of Zn_i.

The 3d transition metal-doped ZnO has already been investigated largely as DMS system over the last two decades. For the generalization of a model for the DMS system, it is better to avoid elements that are magnetic at room temperature, such as Fe, Co and Ni. RE transition metal-doped ZnO has also been studied as DMS system by many research groups. Gd-doped GaN exhibiting RTFM has been reported by Shvarkov *et al* [29]. RTFM in Gd-doped ZnO in various methods was reported [30–33]. Neither Gd nor its clusters with Zn are ferromagnetic at room temperature.

Published online: 05 October 2021

Hence, ZnO with dilute Gd doping is considered as a suitable system for DMS.

In this article, pristine- and Gd-doped (0.05, 0.1 and 1 at%) ZnO films grown on Si(111) substrate by radio frequency magnetron sputtering under pure Ar atmosphere are discussed. Native defects (V_O and Zn_i) are introduced in Gd-doped ZnO films to enhance ferromagnetism with the objective of investigating its effect on the magnetic properties of the films. We have proposed a mechanism that could be responsible for RTFM in Gd-doped ZnO thin film based on BMP model due to oxygen deficiency related defects manifested as V_O and Zn_i [34].

2. Materials and methods

The sputtering targets of ZnO and Gd-doped ZnO (0.05, 0.1 and 1 at%) were prepared using ZnO and Gd_2O_3 powders (Alfa Aesar) with 99.99% purity by conventional solid-state reaction method. The powders were mixed in stoichiometric ratio and ball milled for 10 h followed by calcination for 30 min at 950°C. The ceramic targets prepared using hydraulic pelletizer were sintered for 6 h at 950°C. After attaining vacuum condition (10^{-6} mbar pressure) in the chamber, Gd-doped ZnO thin films were deposited on Si(111) substrate under Ar pressure of 0.02 mbar using the prepared ceramic targets as discussed above. The substrate temperature, RF power and deposition time were maintained as 450°C, 120 W and 30 min, respectively, for all films.

The structural properties of the fabricated films were studied using X-ray diffraction method (XRD) and Raman spectroscopy. XRD analysis was carried out with X-ray diffractometer (Rigaku/Smartlab XRD) using CuK_α source (λ = 1.54 Å). Raman analysis was carried out with Horiba/Lab RAM HR (excitation wavelength = 532 nm). Atomic force microscopy (AFM, Bruker/Dimension Icon) images of the films were recorded for morphological analysis. Elemental analysis was done using X-ray photoelectron spectroscopy (XPS, Kratos/Axis Ultra DLD). Room temperature photoluminescence (PL, Perkin Elmer Ls55) was performed using Xe-lamp of wavelength 325 nm as an excitation source. The magnetic properties of the films were analysed using vibrating sample magnetometer (VSM-Lakeshore 7404) at room temperature. The thickness of the thin films was measured using the Filmetrics F20 system. The thickness of the 1 at% Gd-doped ZnO thin films grown at $Ar:O_2$ = 100:0, 75:25 and 50:50 are 300, 260 and 227 nm, respectively. The thicknesses of 0, 0.05, 0.1 and 1 at% Gd-doped ZnO thin films deposited under pure Ar atmosphere are 280, 274, 267 and 300 nm, respectively.

It is important to mention that 1 at% Gd-doped ZnO thin film was deposited at three different $Ar:O_2$ ratios (100:0,75:25 and 50:50), as preliminary study before growing different concentrations of Gd-doped ZnO films under pure Ar atmosphere. The film grown under pure Ar atmosphere showed RTFM, whereas the films deposited at other oxygen partial pressures exhibited a combination of diamagnetic and ferromagnetic properties. The discussion on the properties of these films is restricted to PL and VSM, as it is beyond the scope of this article.

3. Result and discussion

3.1 *Structural analysis (XRD and Raman spectroscopy)*

Crystal structure of the deposited films was studied using XRD patterns and the obtained XRD patterns are shown in figure 1. The observed peaks of pristine and Gd-doped ZnO films corresponding to the diffraction plane (002) show that all the films are grown with the c-axes perpendicular to the substrate surfaces. This confirms the wurtzite crystal structure of ZnO consistent with JCPDS card #36-1451. The XRD peak at an angle 34.51° for pure ZnO is found to have shifted to lower angles (34.37°, 34.41° and 34.42°) upon doping with Gd (0.05, 0.1 and 1 at%). This shows that the Gd^{3+} ions successfully occupied the lattice sites of Zn^{2+}. Since the ionic radius of Gd^{3+} is 0.93 Å, which is larger than that of Zn^{2+}(0.74 Å), strain was developed in the lattice, causing a shift of peak to a lower angle [30]. When the doping percentage was increased beyond 0.05 at%, the substitutional Gd^{3+} presumably formed complexes with defects. This might be the responsible factor behind the shifting of angle to higher values than that corresponding to 0.05 at% doping [35].

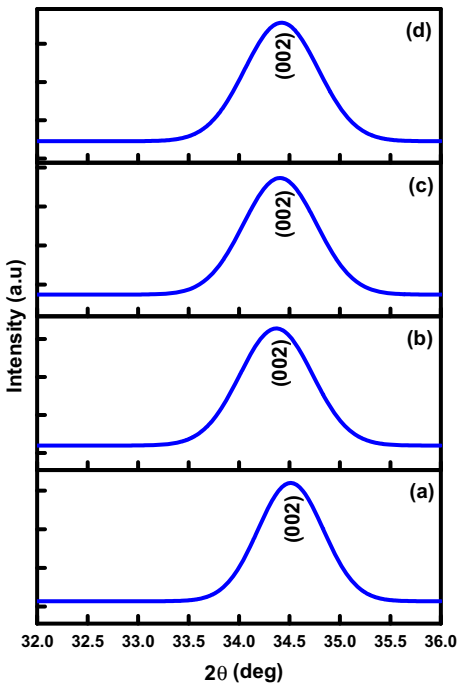

Figure 1. XRD pattern of ZnO with Gd doping percentage of (**a**) 0, (**b**) 0.05, (**c**) 0.1 and (**d**) 1 at%.

The crystallite size was calculated using Scherrer's formula, as given below,

$$D = \frac{k\lambda}{\beta \cos\theta}, \tag{1}$$

where D is the crystallite size, λ the wavelength of CuK_α radiation (1.54 Å), β the full-width at half-maximum of 002 peak in XRD, θ the Bragg's angle and k the shape factor. The lattice parameter 'c' was calculated using the following relation [14],

$$c = \frac{\lambda}{\sin\theta}, \tag{2}$$

where λ is the wavelength of CuK_α radiation (1.54 Å) and θ the Bragg's angle.

The interplanar distance (d) of (002) planes was calculated using the following formula,

$$\frac{1}{d^2} = \frac{h^2 + hk + k^2}{a^2} + \frac{l^2}{c^2}, \tag{3}$$

where h, k and l are the miller indices of the corresponding peaks, a and c are the lattice parameters. The lattice constant a was calculated using the c/a ratio for wurtzite structure

$$\frac{c}{a} = \sqrt{\frac{8}{3}}, \tag{4}$$

where a and c are lattice constants. The crystallite size, D, lattice parameters, a and c, and interplanar distance of (002) planes, d_{002}, are shown in table 1. Crystallite size has been found to vary approximately between 10.9 and 9.7 nm. It is seen that the crystallite size of Gd-doped ZnO is less than that of pure ZnO. The lattice parameter a and c increased after doping with Gd in ZnO. The reduction in crystallite size after doping with Gd can be attributed to the distortion in ZnO structure [30].

Raman spectra of ZnO and Gd-doped ZnO films recorded between 50 and 900 cm^{-1} with an excitation wavelength of 532 nm are shown in figure 2. Wurtzite ZnO belongs to the space group C_{6V}. The primitive cell of ZnO has 2 zinc atoms and 2 oxygen atoms. Hence, at the Γ point of the Brillouin zone, optical phonons have the symmetries, $A_1+2B_1+E_1+2E_2$ [36]. The $2B_1$ symmetry modes are not Raman active. Both polar A_1 and E_1 branches split into longitudinal optical (LO) and transverse optical (TO) modes. E_2 modes are nonpolar and have two frequencies, E_2 (low) and E_2 (high). The E_2 (low) mode predominantly involves vibrations of heavy Zn sublattice, while E_2 (high) mode involves vibrations of lighter O sublattice. For the undoped and Gd-doped ZnO thin films grown on Si(111) substrate, Raman peaks were observed at 98.41, 437.31 and 579.80 cm^{-1}, which correspond to E_2 (low), E_2 (high) and E_1 (LO), respectively. The E_1 (LO) peak at 579.80 cm^{-1} is associated with the defects in the ZnO films [37,38], which may be due to V_O and Zn_i in the films. The intensity of E_2 (high) and E_2 (low) modes indicate the crystallization of ZnO crystal structure [38,39]. The intensity of E_2 (high) and E_2 (low) peaks are found to decrease with the increase in Gd concentration, which shows the restraint degree of crystallisation. Other peaks observed are due to the Si(111) substrate. Kumar *et al* [40] observed that, in Er-doped ZnO synthesized by solid-state reaction method, peaks attributed to Er_2O_3 appear, in addition to peaks corresponding to ZnO. However, in our results, the same peaks observed in pure and Gd-doped ZnO thin films confirm the absence of any secondary structures due to Gd doping.

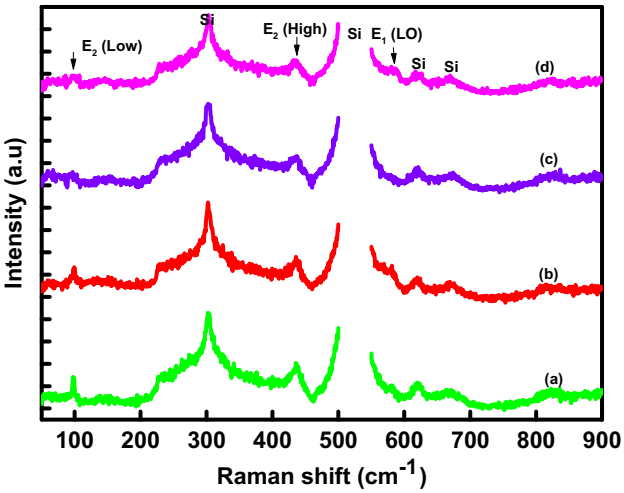

Figure 2. Raman spectra in the range 50–900 cm^{-1} of ZnO with Gd doping percentage of (**a**) 0, (**b**) 0.05, (**c**) 0.1 and (**d**) 1 at%.

3.2 *Morphological analysis (AFM)*

The surface roughness of a thin film is an important parameter for better device fabrication. It influences the electrical conductivity, optical properties [8], structural

Table 1. Crystallite size D, lattice parameter c and interplanar distance d_{002} of (002) planes corresponding to different Gd doping percentages.

Gd doping percentage (at%)	Crystallite size, D (nm)	Lattice constant, c (Å)	Lattice constant, a (Å)	d_{002} (Å)
0	10.9	5.192	3.179	2.596
0.05	9.8	5.214	3.193	2.607
0.1	9.8	5.208	3.189	2.604
1	9.7	5.207	3.188	2.604

integrity and mechanical reliability [41] of the film. For practical devices in spintronics applications, it is important to have low roughness value for thin films. The morphology and surface roughness of the films were studied by AFM analysis. The images were reconstructed on the 5 μm × 5 μm field scan area. It is observed from the AFM images shown in figure 3 that the grains are distributed throughout the surface of the substrate homogeneously and compactly. The root mean square roughness (R_q) values are displayed in table 2. It is seen that 1 at% Gd-doped ZnO thin film shows the lowest roughness value.

Table 2. Root mean square average of roughness (R_q) values corresponding to different Gd doping percentages.

Gd doping percentage (at%)	R_q (nm)
0 at	16.1
0.05	21.64
0.1	7.056
1	3.5

3.3 *Elemental analysis (XPS)*

X-ray photoelectron spectroscopy reveals the electronic states of elements present in the sample. Survey spectrum and high-resolution spectra corresponding to each element in the films were recorded. Calibration of the binding energy was done using the *C* 1s adventitious carbon layer on the surface of the sample. The binding energies corresponding to the peaks obtained in the spectra were compared with the existing literature database (NIST database). The wide scan spectrum of 1 at% Gd-doped ZnO film given in figure 4a shows the presence of zinc, oxygen and gadolinium in addition to adventitious carbon. The corresponding high-resolution spectra of Gd resolved into Gaussian components are shown in figure 4b. The spin-orbit

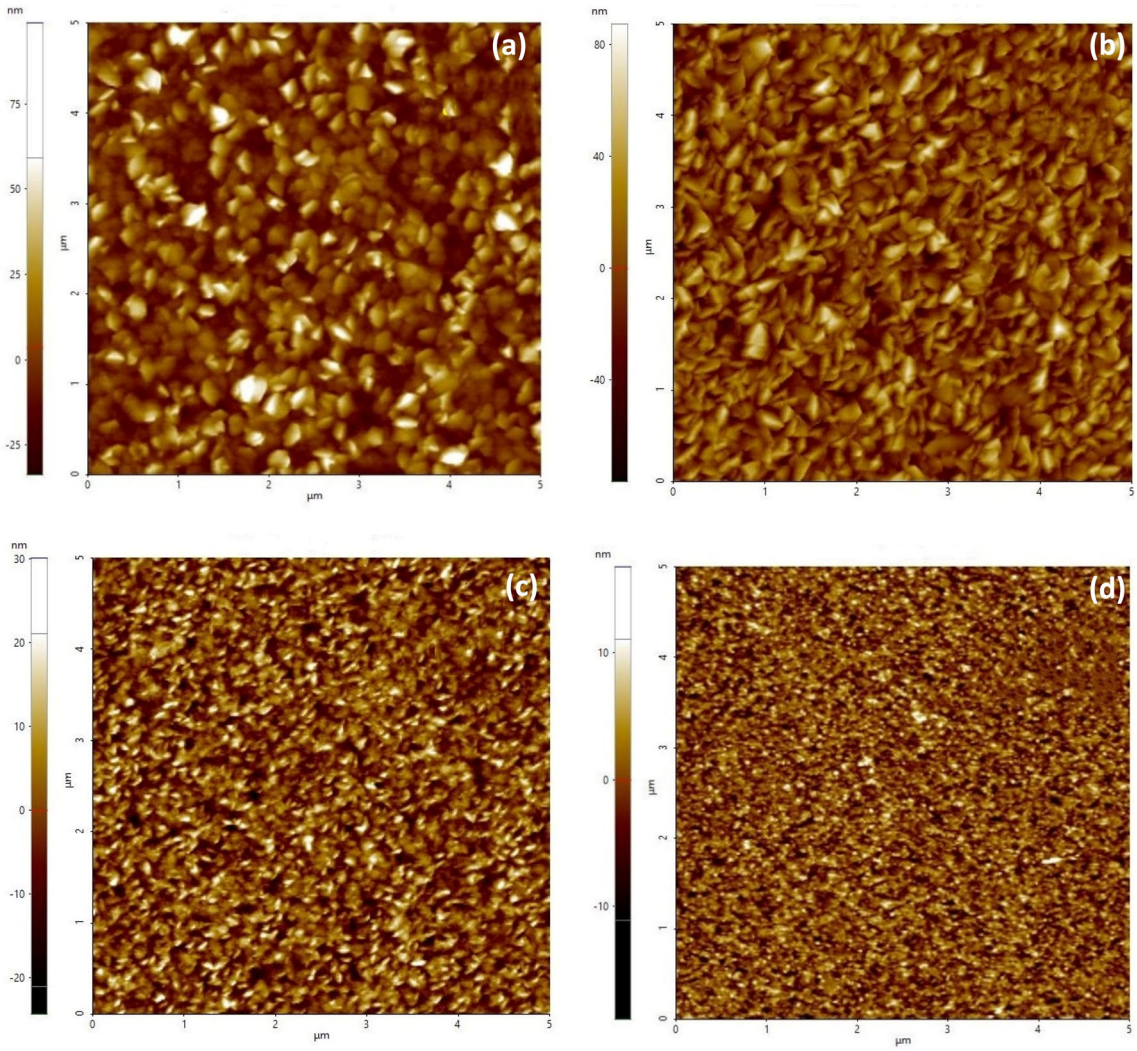

Figure 3. 2D AFM images of ZnO with Gd doping percentage of (**a**) 0, (**b**) 0.05, (**c**) 0.1 and (**d**) 1 at%.

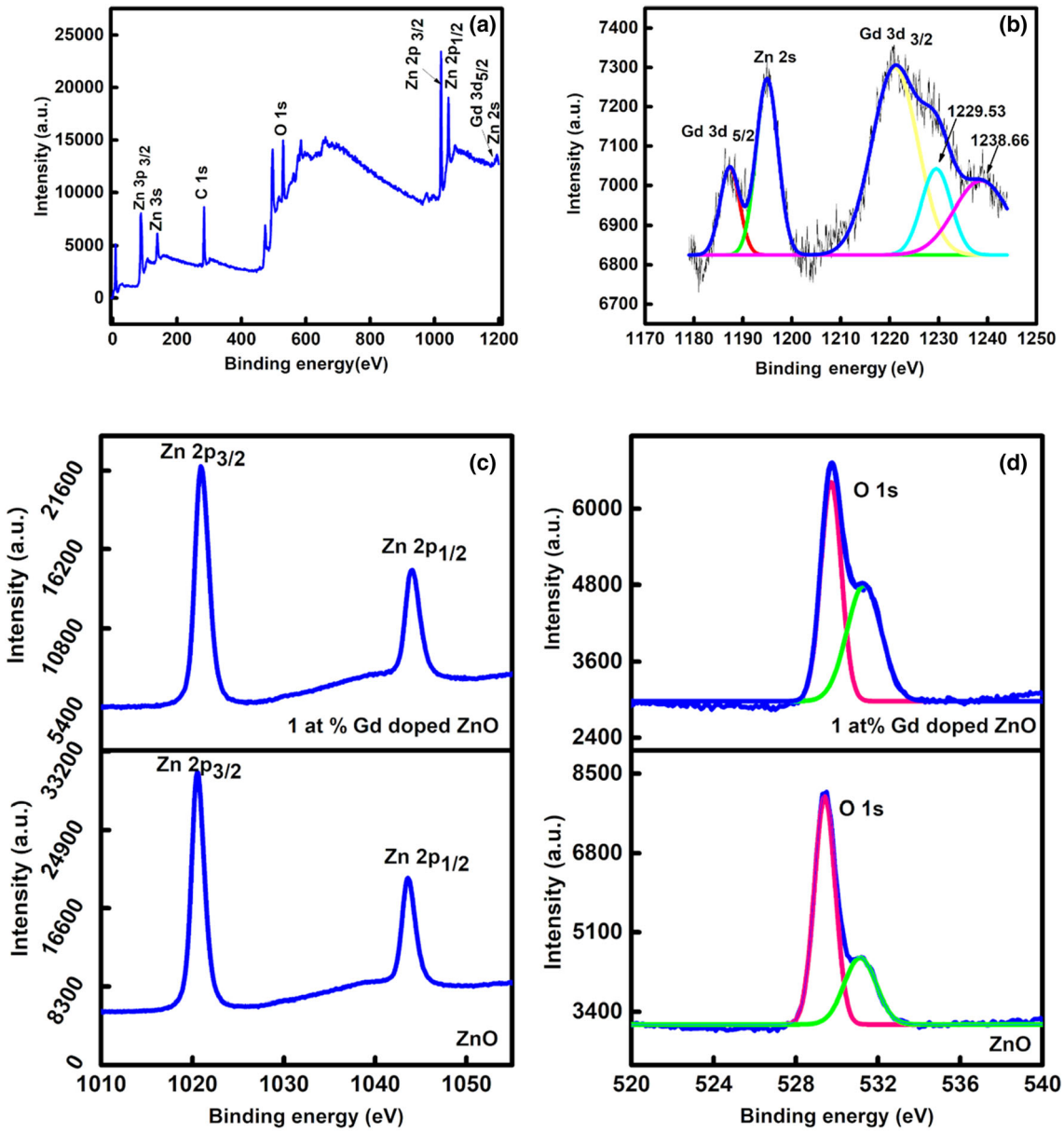

Figure 4. (**a**) Wide spectra of 1 at% Gd-doped ZnO. (**b**) High-resolution spectra of Gd in 1 at% Gd-doped ZnO. (**c**) Zn 2p spectra of ZnO and 1 at% Gd-doped ZnO. (**d**) O 1s spectra of ZnO and 1 at% Gd-doped ZnO.

split doublet is located at 1187.32 and 1221.06 eV for Gd $3d_{5/2}$ and Gd $3d_{3/2}$, respectively, which matches with that of Gd in Gd_2O_3. This shows that Gd exists in the sample in 3+ state. Two satellite peaks of Gd $3d_{3/2}$ are found at 1229.53 and 1238.66 eV, respectively [42]. The peak at 1194.94 eV corresponds to Zn 2s [43]. The O 1s high-resolution spectra of pure ZnO and 1 at% Gd-doped ZnO are shown in figure 4d. O 1s peak is deconvoluted into two Gaussian peaks at 529.5 and 531.2 eV. The first peak is attributed to the oxygen atoms associated with Zn atoms in the wurtzite structure [44]. The second peak is attributed to the O^{2-} ions that are in the oxygen deficient region [44]. Relative ratios of peaks attributed to oxygen vacancy and the Zn-O bonding is increased in 1 at% Gd-doped ZnO thin film. This shows that the Gd doping introduced more oxygen vacancies in the film. In the high-resolution spectrum of Zn 2p in ZnO and 1 at% Gd-doped ZnO given in figure 4c, two peaks are found. The two peaks at 1020.6 and 1043.6 eV correspond to the binding energies of Zn $2p_{3/2}$ and Zn $2p_{1/2}$, respectively, which show 2+ electronic state of Zn.

3.4 *Optical analysis (PL spectroscopy)*

Photoluminescence spectra of the fabricated films were recorded to investigate the structural defects such as atomic

and ionic vacancies, interstitials and substitutions. Figure 5 shows the PL spectra of 1 at% Gd-doped ZnO thin films grown at different oxygen partial pressures. The broad peak at around 2.7 eV in the PL spectra of 1 at% Gd-doped ZnO thin films is due to the presence of Zn_i and V_O in the films. Peaks centred at around 3.2 eV in all the spectra corresponding to the near band edge (NBE) transition is attributed to electron–hole recombination between the conduction band and the valence band. It has been observed that the relative intensities of peaks corresponding to visible (blue and green) emissions and NBE transition (I_{vis}/I_{NBE}) are decreasing with the increase in oxygen partial pressure, which shows that the oxygen deficiency related defects are reduced as oxygen partial pressure is increased. In other words, the film grown under pure Ar atmosphere has more native defects.

PL spectra of 0, 0.05, 0.1 and 1 at% Gd-doped ZnO films are shown in figure 6. A broad peak was found at 2.0 eV, which corresponds to the transition of an electron from the conduction band to a deep level of doubly ionized oxygen vacancy. The red emission at 1.65 eV corresponds to the transition from zinc interstitial to doubly ionized oxygen vacancy [45]. The PL spectra in the range of 1.4 to 4 eV do not show any changes with varying concentrations. However, when the spectra are plotted between 2.4 and 3.4 eV, the difference is evident and is shown in figure 7. The PL spectra in the range 2.4 to 3.4 eV were deconvoluted into 4 peaks by Voigt function. The peak at 3.01 eV corresponds

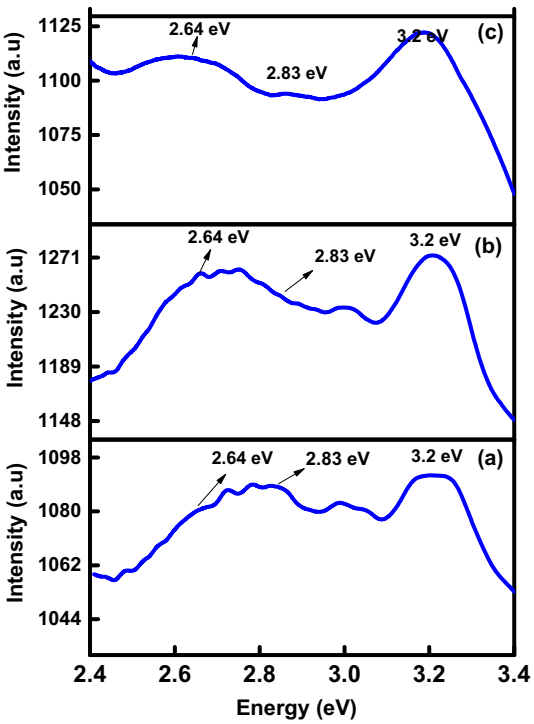

Figure 5. PL spectra in the energy range from 2.4 to 3.4 eV of 1 at% Gd-doped ZnO under Ar:O_2 ratio of (**a**) 100:0, (**b**) 75:25 and (**c**) 50:50.

to weak violet emission due to the transition of an electron from zinc interstitial to valence band [45]. At 2.83 eV, all spectra show peaks that correspond to blue emission, which is a resultant of recombination between the electrons localized at the extended interstitial zinc and holes in the valence band [45]. The peak at 2.64 eV corresponds to blue-green emission due to electron transition from singly ionized oxygen vacancy to valence band [46]. Thus, the study confirms that pure Ar atmosphere growth condition results in more oxygen deficiency in films, which is manifested in the form of V_O and Zn_i [34]. These two are the most stable defects found in ZnO [47]. A small increase in I_{blue}/I_{NBE} and I_{red}/I_{NBE} with the increase in Gd doping percentage was observed from the analysis of PL spectra, which shows that the Zn_i and V_O defects are increased slightly by Gd doping. It might be due to structural disorders created by ionic size mismatched Gd atoms as opposed to Zn in the ZnO lattice [45].

3.5 *Magnetic analysis (VSM)*

The magnetization measurement has been carried out for Si(111) substrate alone at room temperature using vibrating sample magnetometer, and then, performed for Gd-doped ZnO films on Si(111) substrate. The magnetization data of thin films were corrected by subtracting the diamagnetic response of Si(111) substrate. *M–H* loop of 1 at% Gd-doped ZnO thin films deposited at different oxygen partial pressures are shown in figure 8. It is worthy to note that film deposited at Ar:O_2 = 100:0 condition exhibited RTFM, and at other oxygen partial pressures, films exhibited a mix of diamagnetic and ferromagnetic nature. This preliminary study is the driving force to investigate the effect of Gd-doped ZnO films in pure Ar atmosphere as mentioned earlier.

M–H loop of deposited ZnO thin films doped with different concentrations of Gd in Ar atmosphere is given in figure 9. ZnO films with 0.1 and 1 at% percentage Gd shows ferromagnetic nature with saturation magnetization (M_s) values of 3.29 and 4.83 emu cm^{-3}, respectively. The total magnetic moment per Gd is estimated to be 2.71 and 0.4 μ_B per Gd, respectively, for 0.1 and 1 at% Gd-doped ZnO (summarized in table 3). Hence, Ruderman–Kittel–Kasuya–Yosida (RKKY) exchange interaction cannot explain the mechanism for magnetism here, as RKKY interaction will result in a large value of magnetic moment per Gd [48]. The doping percentages chosen here are far less than the percolation threshold of ZnO. Since the distance between Gd^{3+} ions is higher than the lattice constant of ZnO, the mechanism related to super-exchange is not applicable here. Moreover, Gd is in its only oxidation state 3^+ as evident from XPS studies. Hence, the double-exchange mechanism also could not explain the magnetic properties observed [21]. By analysing the PL and magnetic studies of 1 at% Gd-doped ZnO thin films at different

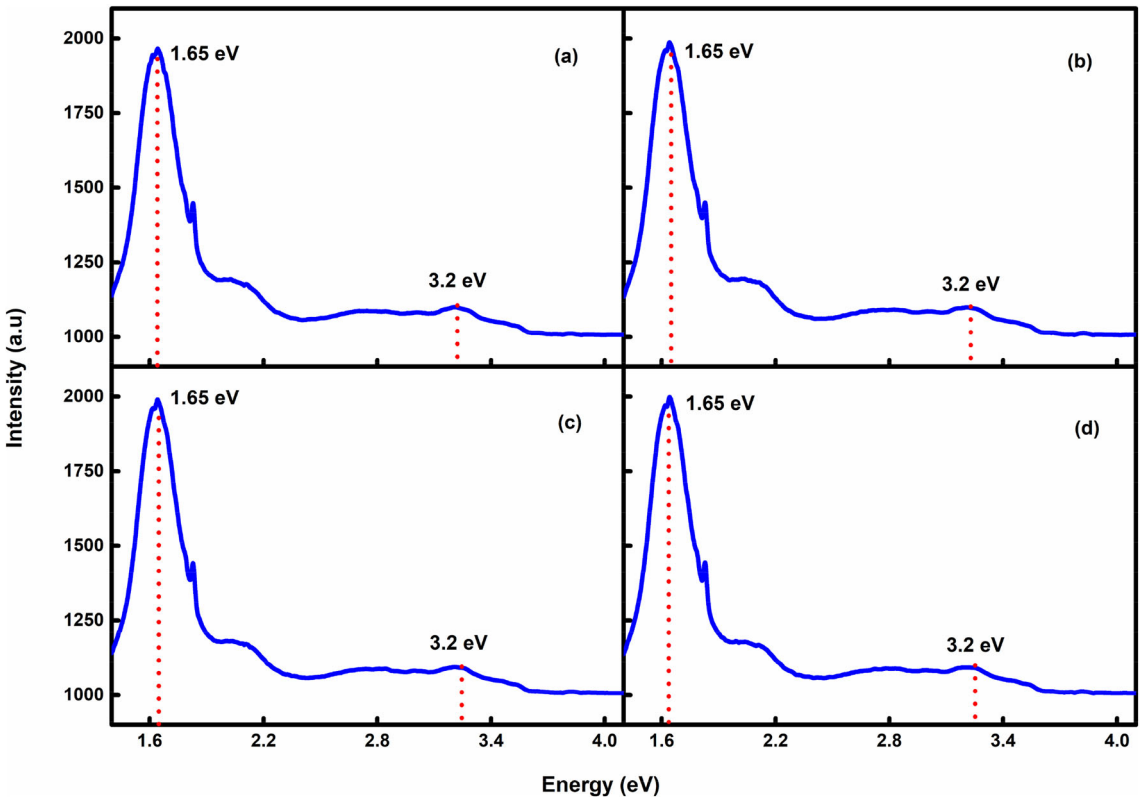

Figure 6. PL spectra ZnO films in the range of 1.4 to 4 eV for Gd doping percentage of (**a**) 0, (**b**) 0.05, (**c**) 0.1 and (**d**) 1 at%.

oxygen partial pressures, it becomes clear that the oxygen deficient condition that caused the formation of a critical amount of V_O or Zn_i defect is responsible for RTFM. The magnetic study reveals that the pure ZnO film exhibits diamagnetic nature. This demonstrates that the lattice defect is not the only reason for RTFM in Gd-doped ZnO system. It also points out that the ferromagnetism induced in other films is not due to the presence of any magnetic impurities. The 0.05 at% Gd-doped ZnO film shows a mixture of diamagnetic and ferromagnetic nature. With further increase in Gd doping concentration, the ferromagnetic property was realized. Hence, it can be inferred that the Gd doping has certainly induced RTFM when the oxygen deficiency related defects are in sufficient numbers. Roqan *et al* [47] and Venkatesh *et al* [33] suggested that defects related to oxygen deficiency–Gd complex mediate ferromagnetism in Gd-doped ZnO systems. Aravindh *et al* [49] used density functional theory to show that Gd-doped ZnO nanowire exhibits RTFM due to s-f coupling when oxygen vacancy is present in it. Vijayaprasath *et al* [50] observed that RE transition metal-doped ZnO shows ferromagnetism due to s-f coupling between RE ions and ZnO host states in the presence of oxygen vacancy and zinc interstitials. In the case of Gd-doped ZnO thin films, Roqan *et al* [51] have proven by DFT calculation that ferromagnetism through s-f or s-d coupling is not possible because the f state is far from the conduction band minimum and does not overlap with the Fermi level. Hence, the possibility of RTFM due to s-f coupling is ruled out in our samples. There is a lot of literature suggesting that V_O and Zn_i together contribute to RTFM in ZnO [52–54]. Although some of the literature points out which of the above defects is dominating in each case, the exact contribution of each defect to the magnetic properties goes unmentioned. Oxygen vacancies in the state of V_O^{++} carry no trapped electron and hence V_O^{++} could not be responsible for ferromagnetism in Gd-doped ZnO films [16]. Now, we are left with Zn_i^+ and V_O^+. Either of the two or both together play a role in ferromagnetism mechanism along with the Gd^{3+} ions. From the PL analysis, Zn_i^+ appears to be the dominant defect, which is a shallow donor defect formed by the Frenkel reaction [55],

$$Zn_{Zn} \Longleftrightarrow Zn_i^* + V_{Zn} \tag{5}$$

Further, electron transition occurs from Zn_i to conduction band and Zn_i^+ is generated.

$$Zn_i^* \Longleftrightarrow Zn_i^+ + e^- \tag{6}$$

This donor electron remains weakly bound to the defect state Zn_i^+ and thus is confined to a hydrogenic orbital with large Bohr radius [56]. When the donor concentration reaches the critical value, these hydrogenic orbitals form an impurity band [21]. These donor electrons interact with Gd^{3+} to form

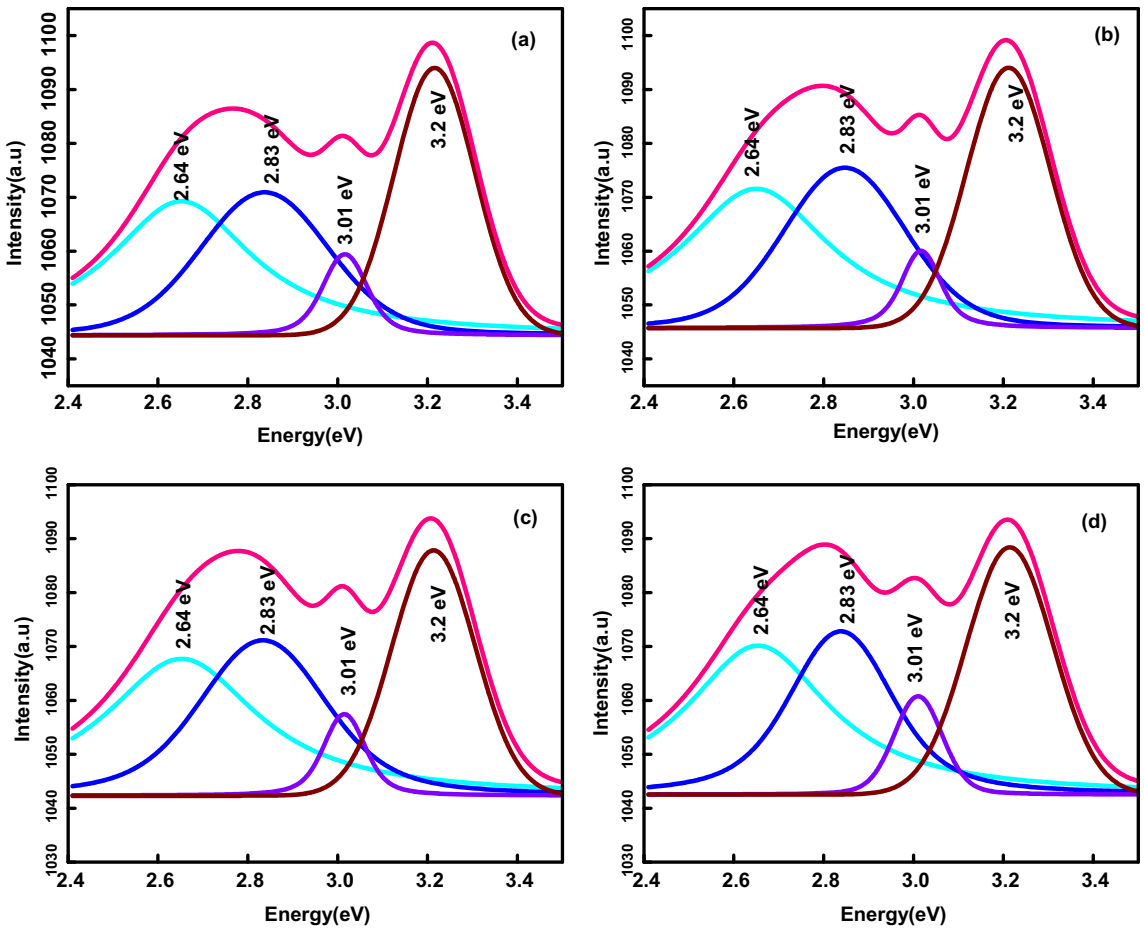

Figure 7. Deconvoluted PL spectra of ZnO films in the range of 2.4 to 3.4 eV for Gd doping percentage of (**a**) 0, (**b**) 0.05, (**c**) 0.1 and (**d**) 1 at%.

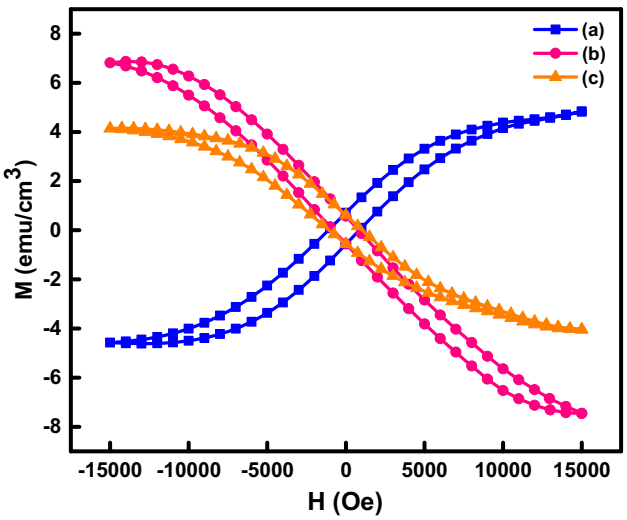

Figure 8. *M–H* loop of 1 at% Gd-doped ZnO grown under Ar:O_2 ratio of (**a**) 100:0, (**b**) 75:25 and (**c**) 50:50.

BMPs. When the number of BMPs is above the BMP percolation threshold of ZnO, they overlap with one another and the spins of Gd^{3+} get into parallel alignment.

Also, V_O^+ is formed by Schottky reaction in the ZnO lattice [57],

$$0 \Longleftrightarrow V_{Zn}^{*} + V_O^{*} \tag{7}$$

$$V_O^{*} \Longleftrightarrow V_O^{+} + e^{-} \tag{8}$$

The donor electron associated with V_O^+ is locally trapped in the hydrogenic orbital formed by V_O^+. The donor electron forms an impurity band when it reaches the critical value. These hydrogenic electrons also interact with Gd^{3+} ions to contribute to the formation of BMP. Thus, ferromagnetism is set by magnetic coupling between inter Gd^{3+} ions mediated by oxygen deficiency related defects (Zn_i^+ and V_O^+).

It is observed that even when Zn_i^+ and V_O^+ are present, pure ZnO thin film grown does not exhibit RTFM. Gd is in +3 state, and its electronic configuration is [Xe] $4f^7$. Hence, the effective coupling between two Gd^{3+} ions in the same donor orbital is ferromagnetic [21]. When the atomic percentage of Gd is 0.05, although ferromagnetism appears, the diamagnetic contribution from ZnO dominates as the number of Gd^{3+} is too low to establish long-range RTFM. This results in a system with a mixture of diamagnetic and

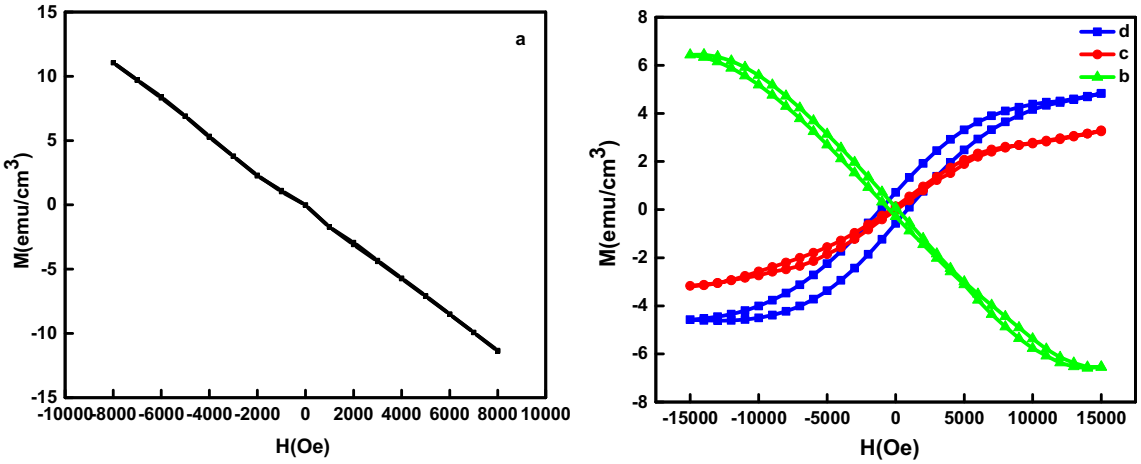

Figure 9. VSM of ZnO with Gd doping percentage of (**a**) 0, (**b**) 0.05, (**c**) 0.1 and (**d**) 1 at%.

Table 3. Magnetic saturation value of ZnO for different Gd doping percentages.

Gd doping percentage (at%)	Magnetic saturation (emu cm^{-3})	Magnetic saturation (μ_B per Gd)
0.1	3.29	2.71
1	4.83	0.40

ferromagnetic nature. When the doping percentage is increased, more Gd^{3+} ions are accommodated inside the hydrogenic orbital associated with the defect, which gives rise to long-range ferromagnetic order in 0.1 and 1 at% Gd-doped ZnO.

The effective magnetic moment per Gd is more for 0.1 at% Gd-doped ZnO compared to 1 at% Gd-doped ZnO. The effective magnetic moment of one Gd^{3+} ion in the sample is 7.9 μ_B calculated from the following equation [58],

$$\mu_{\text{eff}} = g\mu_B[J(J+1)]^{\frac{1}{2}}, \tag{9}$$

where g is Landé g factor, μ_B is Bohr magneton value and J the total angular momentum quantum number. For lower doping percentages of Gd, the effective magnetic moment per Gd should approach this value. The number μ_B/Gd^{3+} in the prepared samples was calculated using the following relation [59],

$$n_{\text{eff}} = \frac{\text{Saturation magnetization}}{(\text{Bohr magneton}) * (\text{number of magnetic atoms per unit volume})} \tag{10}$$

Due to large ionic radii of Gd^{3+} ion (0.93 Å) compared to that of Zn^{2+} ion (0.74 Å), only a lesser number of Gd^{3+} ions presumably occupied the Zn^{2+} sites. Another assumption taken was that all of the Gd^{3+} ions occupied at Zn^{2+} sites contribute to ferromagnetism, which may not be true in the actual case. There could be uncoupled Gd ions. Hence, the calculated M_s value for 0.1 at% Gd-doped ZnO is 2.71 μ_B per Gd [60,61]. When the doping percentage of Gd in ZnO is increased to 1 at%, the magnetic moment per Gd^{3+} decreases to 0.40 μ_B per Gd. Number of magnetic atoms per unit volume in 1 at% Gd-doped ZnO is expected to be 10 times higher than that in 0.1 at% Gd-doped ZnO. However, the M_s values in units of emu cm^{-3} did not increase proportionally corresponding to the doping concentration, because (i) some Gd^{3+} ions would have moved to interstitial positions, and (ii) all Gd^{3+} ions at Zn^{2+} sites are not coupled ferromagnetically. Thus, interstitial Gd^{3+} ions, presence of uncoupled Gd^{3+} ions at Zn^{2+} sites and large ionic radius all together cause the large deviation from the expected effective magnetic moment per Gd^{3+}.

The measured magnetization of 1 at% Gd-doped ZnO and 0.1 at% Gd-doped ZnO are fitted to the relation given below to find out the number of BMPs [62],

$$M = M_0 L(x) + \chi_m H, \tag{11}$$

Here, $M_0 = Nm_s$, where N is the number of BMPs in the sample and m_s the magnitude of the aligned spontaneous magnetic moment of single BMP. $L(x)$ is the Langevin function with $x = \frac{m_{\text{eff}}H}{k_B T}$, where k_B is the Boltzmann constant and m_{eff} the effective spontaneous magnetic moment per BMP. χ_m is the susceptibility of the matrix. So, the first term in the equation represents BMP contribution and the second term, the matrix contribution. On fitting with the above equation, the number of BMPs in 1 and 0.1 at% Gd-doped ZnO thin films are estimated to be 5.233×10^{17} and 1.5485×10^{17} cm^{-3}, respectively, which is higher than the BMP percolation threshold for ZnO (1.5×10^{-3} cm^{-3}) [21]. The BMP fit has been given in figure 10.

There must be a critical number of carriers that would have caused the overlapping of 1s orbitals of electron associated with the oxygen deficiency related defects, which further leads to the formation of BMP. According to BMP model, this critical number of carriers should be in the order of 10^{19} cm^{-3} for ZnO [21,63]. The presence of Zn_i and V_O clearly shows that all the samples prepared are *n* type. According to BMP model, it is expected that the donor electron concentration must be in the range of 10^{19} cm^{-3} or above for 0.1 and 1 at% Gd-doped ZnO thin films grown at oxygen deficient conditions.

From our analysis, it is evident that the oxygen deficient condition favours ferromagnetism. There are two prerequisite conditions for the film to exhibit RTFM, namely, (1) oxygen deficiency related defects in +1 oxidation state in sufficient number so that the BMPs percolate, and (2) an appropriate amount of Gd doping for the film. Under these conditions, the M_s value will vary with Gd concentration.

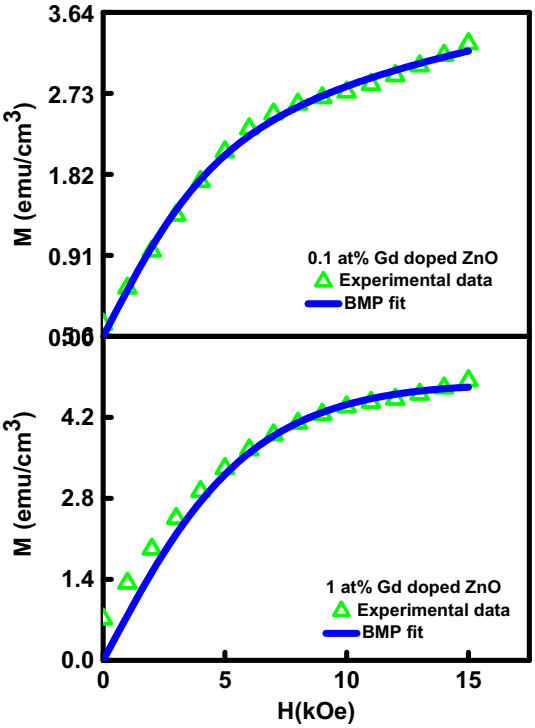

Figure 10. Fit of the *M–H* curve with BMP model for 0.1 and 1 at% Gd-doped ZnO.

4. Conclusion

In this article, the effect of Gd on ZnO thin films in pure Ar ambience was investigated to realize ferromagnetism. As part of the investigation, 1 at% Gd-doped ZnO thin film was deposited at different Ar:O_2 ratios (100:0, 75:25 and 50:50) on Si(111) substrate. The film deposited under oxygen deficient condition (pure Ar) exhibited RTFM, whereas the films deposited at other oxygen partial pressures exhibited a mixture of diamagnetism and ferromagnetism.

Based on this preliminary investigation, different concentrations (0, 0.05, 0.1 and 1 at%) of Gd-doped ZnO films were grown under pure Ar atmosphere to introduce more native defects (V_O, Zn_i). The structural, morphological, elemental, optical and magnetic properties were analysed. It has been found that for 0.1 and 1 at% Gd-doped ZnO films exhibit long-range RTFM as the critical amount of Zn_i^+ and V_O^+, and the appropriate amount of Gd^{3+} ions exist for these films. These conditions have been investigated and discussed in detail. Pure ZnO has been observed to exhibit diamagnetism. The 0.05 at% Gd-doped ZnO film showed a vortex state, as one of these prerequisite conditions, the appropriate amount of Gd^{3+} ions, had not been satisfied. The values of saturation magnetization for 0.1 and 1 at% Gd-doped ZnO film have been found to be 2.71 and 0.40 μ_B per Gd, respectively. The number of BMPs formed in 0.1 and 1 at% Gd-doped ZnO samples are obtained by BMP fit as 1.5485×10^{17} and 5.233×10^{17} cm^{-3}, respectively, which are well above the BMP percolation threshold of ZnO. It is proved that the appropriate Gd doping along with a sufficient number of oxygen deficiency related defects are required for the system to be ferromagnetic. The magnetic properties of Gd-doped ZnO DMS system are well explained with BMP model based on oxygen deficiency related defects.

Acknowledgements

AS acknowledges MHRD, Government of India, for providing Junior Research Fellowship (JRF) Grant to undertake this research work.

References

[1] Zhang L, Zhu L, Hu L, Li Y, Song H and Ye Z 2016 *RSC Adv.* **6** 57403
[2] Tian Z M, Yuan S L, Yin S Y, Zhang S Q, Xie H Y, Miao J H *et al* 2008 *J. Magn. Magn. Mater.* **320** L5
[3] Ali N, Singh B, Khan Z A, Vijaya A R, Tarafder K and Ghosh S 2019 *Sci. Rep.* **9** 2461

[4] Nallusamy S and Nammalvar G 2018 *Mater. Res. Express* **5** 026418
[5] Xia C, Hu C, Chen P, Wan B, He X and Tian Y 2010 *Mater. Res. Bull.* **45** 794
[6] Alla S K, Kollu P, Mandal R K and Prasad N K 2018 *Ceram. Int.* **44** 7221
[7] Nachiar R A and Muthukumaran S 2019 *Opt. Laser Technol.* **112** 458
[8] Sujatha Lekshmy S, Anitha V S and Joy K 2014 *Mater. Res. Soc. Symp. Proc.* **1675** 113
[9] Cui X G, Tao Z K, Zhang R, Li X, Xiu X Q, Xie Z L *et al* 2008 *Appl. Phys. Lett.* **92** 152116
[10] Seong H K, Kim J Y, Kim J J, Lee S C, Kim S R, Kim U *et al* 2007 *Nano Lett.* **7** 3366
[11] Janotti A and Van De Walle C G 2009 *Rep. Prog. Phys.* **72** 126501
[12] Tao Y M, Ma S Y, Chen H X, Meng J X, Hou L L, Jia Y F *et al* 2011 *Vacuum* **85** 744
[13] Yoon H, Hua Wu J, Hyun Min J, Sung Lee J, Ju J S and Keun Kim Y 2012 *J. Appl. Phys.* **111** 07B523
[14] Fifere N, Airinei A, Timpu D, Rotaru A, Sacarescu L and Ursu L 2018 *J. Alloys Compd.* **757** 60
[15] Arora D, Asokan K, Mahajan A, Kaur H and Singh D P 2016 *RSC Adv.* **6** 78122
[16] Quan Z, Liu X, Qi Y, Song Z, Qi S, Zhou G and Xu X 2017 *Appl. Surf. Sci.* **399** 751
[17] Nie X, Zhang B, Wang J, Shi L, Di Z and Guo Q 2015 *Mater. Lett.* **161** 355
[18] Herng T S, Lau S P, Wei C S, Wang L, Zhao B C, Tanemura M *et al* 2009 *Appl. Phys. Lett.* **95** 13
[19] Wang J, Hou S, Chen H and Xiang L 2014 *J. Phys. Chem. C* **118** 19469
[20] Ogale S B 2010 *Adv. Mater.* **22** 3125
[21] Coey J M D, Venkatesan M and Fitzgerald C B 2005 *Nat. Mater.* **4** 173
[22] Iqbal J, Wang B, Liu X, Yu D, He B and Yu R 2009 *New J. Phys.* **11** 063009
[23] Ahmed S A 2017 *Results Phys.* **7** 604
[24] Li F, Liu X C, Zhou R W, Chen H M, Zhuo S Y and Shi E W 2014 *J. Appl. Phys.* **116** 243910
[25] Pivin J C, Socol G, Mihailescu I, Berthet P, Singh F, Patel M K *et al* 2008 *Thin Solid Films* **517** 916
[26] Zhang X, Wang W H, Li L Y, Cheng Y H, Luo X G, Liu H *et al* 2008 *EPL* **84** 27005
[27] Bin Chen W, Liu X C, Li F, Chen H M, Zhou R W and Shi E W 2015 *AIP Adv.* **5** 067105
[28] Ali N, Vijaya A R, Khan Z A, Tarafder K, Kumar A, Wadhwa M K *et al* 2019 *Sci. Rep.* **9** 20039
[29] Shvarkov S, Ludwig A, Wieck A D, Cordier Y, Ney A, Hardtdegen H *et al* 2014 *Phys. Status Solidi Basic Res.* **251** 1673
[30] Obeid M M, Jappor H R, Al-Marzoki K, Al-Hydary I A, Edrees S J and Shukur M M 2019 *RSC Adv.* **9** 33207
[31] Kaur P, Kumar S, Chen C L, Hsu Y Y, Chan T S, Dong C L *et al* 2016 *Appl. Phys. A* **122** 161
[32] Potzger K, Zhou S, Eichhorn F, Helm M, Skorupa W, Mücklich A *et al* 2006 *J. Appl. Phys.* **99** 063906
[33] Venkatesh S, Franklin J B, Ryan M P, Lee J S, Ohldag H, McLachlan M A *et al* 2015 *J. Appl. Phys.* **117** 013913
[34] Janotti A and Van De Walle C G 2007 *Phys. Rev. B-Condens. Matter Mater. Phys.* **76** 1
[35] Xin M 2018 *J. Theor. Appl. Phys.* **12** 177
[36] Zhou H, Chen L, Malik V, Knies C, Hofmann D M, Bhatti K P *et al* 2007 *Phys. Status Solidi Appl. Mater. Sci.* **204** 112
[37] Wang X, Li Q, Liu Z, Zhang J, Liu Z and Wang R 2004 *Appl. Phys. Lett.* **84** 4941
[38] Zhang M, Averseng F, Haque F, Francia, Borghetti P, Krafft J M *et al* 2019 *Nanoscale* **11** 5102
[39] Lin C C, Young S L, Kung C Y, Horng L, Chen H Z, Kao M C *et al* 2013 *Vacuum* **87** 178
[40] Kumar P, Sharma V, Sarwa A, Kumar A, Surbhi, Goyal R *et al* 2016 *RSC Adv.* **6** 89242
[41] Du L and Maroudas D 2017 *Appl. Phys. Lett.* **110** 103103
[42] Vijayaprasath G, Murugan R, Hayakawa Y and Ravi G 2016 *Lumin. J.* **178** 375
[43] Mithal D and Kundu T 2017 *Solid State Sci.* **68** 47
[44] Hsieh P T, Chen Y C, Kao K S and Wang C M 2008 *Appl. Phys. A Mater. Sci. Process.* **90** 317
[45] Bandopadhyay K and Mitra J 2015 *RSC Adv.* **5** 23540
[46] Wu X, Xu Z, Liu B, Sun T, Zhao W, Liu S *et al* 2014 *Appl. Phys. A Mater. Sci. Process.* **114** 847
[47] Roqan I S, Venkatesh S, Zhang Z, Hussain S, Bantounas I, Franklin J B *et al* 2015 *J. Appl. Phys.* **117** 073904
[48] Ma X 2012 *Thin Solid Films* **520** 5752
[49] Aravindh S A, Schwingenschloegl U and Roqan I S 2014 *J. Appl. Phys.* **116** 1
[50] Vijayaprasath G, Murugan R, Mahalingam T, Hayakawa Y and Ravi G 2015 *Ceram. Int.* **41** 10607
[51] Roqan I S, Aravindh S A and Venkatesh S 2016 in M Khan (ed) *Magnetic materials* (IntechOpen) 251 https://www.intechopen.com/chapters/51165
[52] Li J, Li Y, Li S, Zhu M, Zhang J, Li Y *et al* 2020 *Ceram. Int.* **46** 18639
[53] Olive-Méndez S F, Santillán-Rodríguez C R, González-Valenzuela R A, Espinosa-Magaña F and Matutes-Aquino J A 2014 *Nanoscale Res. Lett.* **9** 1
[54] Gandhi V, Ganesan R, Abdulrahman Syedahamed H H and Thaiyan M 2014 *J. Phys. Chem. C* **118** 9717
[55] Kayaci F, Vempati S, Donmez I, Biyikli N and Uyar T 2014 *Nanoscale* **6** 10224
[56] Ghose S, Rakshit T, Ranganathan R and Jana D 2015 *RSC Adv.* **5** 99766
[57] Zeng H, Duan G, Li Y, Yang S, Xu X and Cai W 2010 *Adv. Funct. Mater.* **20** 561
[58] Nikiforov V N, Kuznetsov V D, Ruchkin A V and Salyanov V I 2005 *Proc. Third Moscow Int. Symp. Magn.* 249
[59] McKeehan L W 1950 *Phys. Rev.* **79** 745
[60] Ali N, Singh B and Ghosh S 2019 *J. Magn. Magn. Mater.* **492** 1
[61] Dakhel A A and El-Hilo M 2010 *J. Appl. Phys.* **107** 123905
[62] Pal B and Giri P K 2011 *J. Nanosci. Nanotechnol.* **11** 9167
[63] Duan L B, Rao G H, Yu J, Wang Y C, Chu W G and Zhang L N 2007 *J. Appl. Phys.* **102** 103907